Materials Science & Engineering A 657 (2016) 6–14

Contents lists available at ScienceDirect

Materials Science & Engineering A

journal homepage: www.elsevier.com/locate/msea

Ultrafine-grained Al composites reinforced with *in-situ* Al_3Ti filaments

Peter Krizik [a,*], Martin Balog [a], Martin Nosko [a], Maria Victoria Castro Riglos [b], Jiri Dvorak [c], Oto Bajana [a]

[a] Institute of Materials and Machine Mechanics, Slovak Academy of Sciences, Racianska 75, 83102 Bratislava, Slovak Republic
[b] Centro Atómico Bariloche, Av. Bustillo 9500 (8400) Bariloche, Río Negro, Argentina
[c] CEITEC-IPM, Institute of Physics of Materials, ASCR, Zizkova 22, 61662 Brno, Czech Republic

ARTICLE INFO

Article history:
Received 21 October 2015
Received in revised form
14 January 2016
Accepted 16 January 2016
Available online 18 January 2016

Keywords:
Aluminum
Filament
in-situ metal matrix composite
Mechanical properties
Microstructure
Ultrafine-grained

ABSTRACT

Ultrafine-grained (UFG) Al matrix composites reinforced with 15 and 30 vol% *in-situ* Al_3Ti filaments were fabricated by extrusion of Al–Ti powder mixtures followed by solid-state reactive diffusion. Fine Al powder particles (1.3 μm) heavily deformed the coarser Ti particles (24.5 μm) into filaments during extrusion. Upon a subsequent operation of hot isostatic pressing (HIP), the micrometric Al_3Ti filaments elongated along the extrusion direction and formed *in situ* in the UFG Al matrix. Fabricated composites are free of pores and voids with perfect bonding created at the Al–Al_3Ti interfaces. In parallel, a small portion (2.4 vol%) of nanoscale γ-Al_2O_3 particles, which originate from native amorphous films on fine Al powders, formed *in situ* and were homogenously dispersed in the Al matrix. The microstructures of as-extruded and after HIP composites were analyzed by means of scanning electron microscopy (SEM), transmission electron microscopy (TEM), X-ray diffraction (XRD), energy dispersive spectrometry (EDS) and electron back-scattered diffraction (EBSD). Owing to the presence of nanometric γ-Al_2O_3 particles with Al high angle grain boundaries (HAGBs), the UFG Al matrix remained stable even after HIP at 600 °C for 9 h. The mechanical properties and creep performance of composites at testing temperatures of up to 600 °C were systematically studied. The Al–Al_3Ti composites exhibited a combination of increased strength and Young's modulus in addition to excellent creep performance and structural stability, which indicates that the studied composites are potential structural materials capable of service at elevated temperatures.

1. Introduction

Aluminum (Al) metal matrix composites (MMCs) strengthened with fiber reinforcement offer a favorable combination of improved physical and mechanical properties and hence represent an interesting group of materials for structural application in the automotive and aerospace industry [1]. However, traditional *ex situ* fabricated Al-MMCs strengthened with ceramic fiber reinforcement suffer from numerous drawbacks, including (i) problematic introduction of the reinforcement, which results in microstructural inhomogeneity and residual porosity; (ii) the damage of reinforcement during hot working techniques; and (iii) the undesired interfacial reaction between the Al matrix and reinforcement, which results in deteriorated properties of the MMCs [2,3]. This stimulated the development of Al-MMCs fabricated *in situ*, where the above-mentioned disadvantages can be avoided to a large extent.

Al_3Ti has one of the highest Young's modulus (YM) among all Al-rich aluminides at 217 GPa [4,5], a relatively low density (ρ) of 3.35 g/cm^3 and a high melting point of 1350 °C [6]. Moreover, assuming a good reactivity of Al with titanium (Ti), Al_3Ti represents an excellent candidate for an *in-situ* reinforcing phase in Al-MMCs, which can provide significant improvement of stiffness, strength and thermal stability. *In-situ* Al–Al_3Ti MMCs are fabricated using various technological approaches, essentially divided into two major routes: (i) preparation in the molten state [7–9] and (ii) solid state preparation using powder metallurgy (PM) techniques [6,10–18]. Fabrication in the molten state involves incorporation and reaction of Ti powder [7] or Ti containing compound [9] in Al melt, or alternatively is realized by stir casting of Ti alloyed Al melt [8]. The solid state fabricated MMCs are produced by sintering of elemental [10] or mechanically alloyed [6, 11–14] Al–Ti powder blends, or by friction stir processing of consolidated material produced from Al–Ti powder mixture [15–17]. The selection of the processing route affects the shape, size, morphology and nature of *in-situ* Al_3Ti reinforcement as well as Al matrix microstructure, with a direct consequence on the mechanical properties of the formed MMCs. Owing to the low diffusivity and solubility of Ti in

* Corresponding author.
E-mail address: peter.krizik@savba.sk (P. Krizik).

http://dx.doi.org/10.1016/j.msea.2016.01.047
0921-5093/

Al [19–21], the Al–Ti reaction is better controlled in the solid state. In addition, Al_3Ti exhibits a low coarsening rate below the melting point of the Al matrix. Therefore, solid state processing yields generally finer and more homogenous microstructures compared to those obtained by casting methods and is therefore the more favorable approach. As a result of the volume changes and the Kirkendall´s phenomenon during the formation of Al_3Ti, solid state processing realized at the atmospheric pressure yields Al–Al_3Ti MMCs with increased residual porosity. Hot isostatic pressing (HIP) is used to reduce the residual porosity, and *in-situ* Al–Al_3Ti MMCs with nearly full density are obtained [21–24]. Though, the minimal temperature of ~520 °C is required for an acceptable reaction of Al with Ti [10, 16, 25]. Long-term exposures at such high reaction temperatures are detrimental to common strengthening mechanism active in Al and Al alloys (e.g., precipitation and solid solution hardening, strengthening by the Al grain boundaries (GBs)). This puts emphasis on the search for suitable strengthening mechanisms, which remains effectively active in *in-situ* Al–Al_3Ti MMCs even after long-term exposures at such high reaction temperatures.

In this study, we report the processing, microstructures, and mechanical properties of a new type of UFG Al-MMC reinforced with *in-situ* Al_3Ti filaments fabricated by direct extrusion (DE) of Al–Ti powder mixtures followed by the solid state reaction by HIP. The employed UFG Al matrix forms by plastic shearing of fine Al powder (d_{50}=1.3 μm) during the DE. The relatively high strength of the UFG Al matrix stems from the mediated strengthening mechanism of the Al GBs [31, 32]. In addition, a small volume fraction of nanometric γ-Al_2O_3 dispersoids, evenly dispersed in the UFG Al matrix, develops as a result of the fragmented, thin (~2.5 nm) native amorphous (am)-Al_2O_3 layers on the Al powder [31–33]. Such UFG Al–Al_2O_3 MMCs, named HITEMAL® (high temperature aluminum), were introduced by Balog et al. [26–33]. The excellent long-term structural stability of HITEMAL® up to 600 °C is due to the pinning effect of the γ-Al_2O_3 phase at GBs [33]. Hence, the strengthening mechanism of the GBs active in the UFG Al matrix is expected to be preserved in Al–Al_3Ti MMCs even after prolonged exposures at high temperatures required for *in-situ* formation of Al_3Ti during HIP. Owing to an excellent thermal stability reported for the *in-situ* Al_3Ti and UFG Al-γ-Al_2O_3 matrix, superior high temperature performance of fabricated Al–Al_3Ti MMCs is expected and assessed in this study.

2. Experimental

Air atomized Al powder (Al ≥ 99.8 wt%) with a median size d_{50} =1.3 μm and hydride–dehydride (HDH) processed Ti powder (Ti ≥ 99.4 wt%) with d_{50}=24.5 μm were used for this study (Fig. 1). A FRITSCH Analysette 22 laser diffraction system by wet dispersion was used to determine d_{50} values. The Al–Ti powder mixtures were blended in a Turbula shaker for 30 min. The powder mixtures contained 4.1 and 8.2 vol% of Ti powder, which represents 15 and 30 vol% Al_3Ti after reaction. Powder mixtures were compacted by cold isostatic pressing (CIP) at 150 MPa. CIP green compacts were subjected to vacuum degassing at 425 °C for 12 h at ~10 Pa vacuum prior to the direct extrusion (DE). Degassed green compacts were extruded at 475 °C with a reduction ratio of 25:1 (the true strain $\eta = 3.2$) and under the ram speed of 0.5 mm s^{-1} using a die 6 mm in diameter. To form the *in-situ* Al_3Ti phase by a solid state reaction between Al–Ti, the extruded samples were processed by HIP at 600 °C for 9 h under argon (Ar) atmosphere and pressure of 150 MPa. For comparison, unreinforced Al matrix was prepared following the same processing procedure as used in the case of Al–Al_3Ti MMCs. The prepared samples are listed in Table 1.

The density of the prepared samples was measured using Archimedes' principle according to the ASTM B962-08 standard. The microstructure of composites was analyzed using SEM (JEOL 7500 machine) equipped with an EBSD detector. Detailed microstructural characterization was performed using TEM (FEI TECNAI G2 machine, 200 kV) that was complemented with an EDS detector. The thin foils were prepared by wire electro discharge machining and mechanical grinding followed by ion milling (Gatan PIPS machine). The average filament thickness was calculated according to the standard stereographic intercept method [34] using SEM. The phase analysis was carried out using XRD (Philips X'Pert machine, Cr Kα radiation).

Tensile specimens with 3-mm diameter and 30-mm gauge length were machined along the longitudinal direction of the extruded materials. The specimens were tested using a Zwick Roell 1474 testing machine at a strain rate of $\sim 5 \times 10^{-4}$ s^{-1} according to the ASTM E8 and ASTM E21 standards. Tensile tests were performed at various temperatures from room temperature (RT) up to 600 °C. The tensile bars were heated up to the desired testing temperature for 20 min and stabilized for 10 minutes prior to starting the high temperature tensile tests. The as-processed materials were annealed at 300 °C for 24 h prior to tensile tests. The tensile properties of each material were measured using at least four samples. The Young's modulus (YM) was determined by dynamical mechanical analysis (DMA, Q600 TA Instruments machine) using 3-point bending tests. For these tests, the samples with dimensions of 2.5x4x55 mm were used. A frequency of 1 Hz, a preload force of 0.5 N and a dynamic force of 7 N were set up for room temperature tests. The YM of each material was measured using two samples, and each sample was measured 4 times on each side. In the case of YM determined at elevated temperatures (from RT to 400 °C), a heating rate of 3 K/min, a preload force of 0.5 N and a dynamic force of 3 N were used. Owing to the

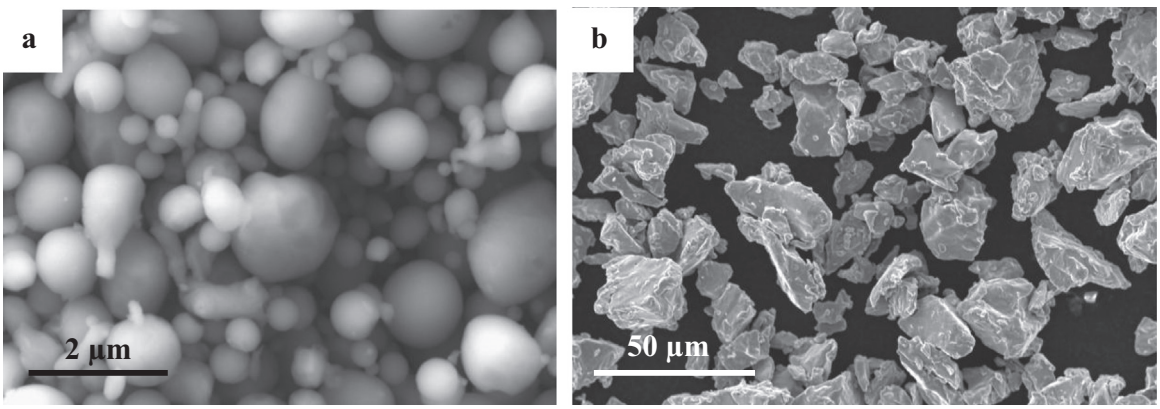

Fig. 1. SEM images of as-received Al (a) and Ti (b) powders.

Table 1
The designation of prepared materials and their porosity.

Designation	Composition	Condition	Ti filament fraction (vol%)	Al_3Ti filament fraction (vol%)	Porosity (%)*
A	UFG_Al	as-extruded	–	–	1
B	UFG_Al_HIP	HIP	–	–	0.5
C	UFG_Al+4.1% Ti_f	as-extruded	4.1	–	1.4
D	UFG_Al+8.2% Ti_f	as-extruded	8.2	–	1
E	UFG_Al+15% Al_3Ti_f	HIP	–	15	0.9
F	UFG_Al+30% Al_3Ti_f	HIP	–	30	0.5

* The theoretical density of the composites was calculated while taking into account that the Al matrix contains 2.4 vol% γ-Al_2O_3 [28].

reproducibility of the results, the temperature dependencies were measured for two samples. For the creep tests, the cylindrical samples with the gauge of 3–35 mm were machined along the longitudinal direction. Creep tests were performed using a lever arm tensile creep testing machine by various applied constant stresses between 30 and 90 MPa. Creep tests were conducted over the temperature range of 250 to 500 °C in Ar. The stress exponent n was calculated from the power-law creep Eq. (1):

$$n = \left(\frac{\partial \ln \dot{\varepsilon}_m}{\partial \ln \sigma} \right)_T \quad (1)$$

where $\dot{\varepsilon}_m$ is the minimum creep rate, σ is the stress, and T is the absolute temperature.

3. Results and discussion

3.1. Microstructure

The extruded unreinforced material A shows small residual porosity of 1%, which is further reduced after HIP (material B) to 0.5% (Table 1). The representative longitudinal and transverse cross-section images of as-extruded Al–Ti composite D are shown in Fig. 2a and b. In spite of a relative low true strain ($\eta = 3.2$) induced during extrusion, the Al powder severely deforms the Ti particles into micrometric filaments oriented parallel to the extrusion direction. At used extrusion temperature the deformation resistance of a fine Al powder is similar or larger compared to a coarser HDH Ti powder. This is attributed to a fine particle size of Al powder with a large surface area and to a high strength of Al matrix (i.e., HITEMAL®) at used extrusion temperature [33]. As a result, Ti powder undergoes a severe shear deformation during extrusion compaction and Ti filaments with a high aspect ratio form eventually. Similar microstructure was observed by Russell et al. [35] in the case of Al–Ti composites deformed with $\eta = 6.8$. Owing to the size of the Al powder and relative low volume content of Ti particles, Ti filaments are uniformly distributed in the Al matrix. Essentially, the thickness of Ti filaments does not change with the content of Ti filaments and is 1.7 and 1.4 μm for C and D composites, respectively (Table 2). Compared to unreinforced matrix materials, the formation of Al–Ti interfaces results in a slight increase in the residual porosity to 1.4 and 1% for C and D composites, respectively (Table 1). Elongated Al matrix grains in C and D have the average transversal grain size of 0.68 ± 0.42 μm as determined by EBSD (Fig. 3). Furthermore, EBSD reveals minor preferential orientation of Al grains (plane {111} parallel with the extrusion direction) and a relatively small portion (10.1%) of low angle grain boundaries (LAGBs, 3–15°). As confirmed by EDS, a thin layer (~200 nm) of the Al_3Ti nano-crystals forms at the interface between Al matrix and Ti filaments (Fig. 4a). This indicates that the onset of the reaction between Al and Ti takes place during DE. TEM reveals two different types of interfaces between adjacent Al powder grains in the matrix area (i.e., powder particles). Al HAGBs are mostly decorated with thin Al_2O_3 layers, which originate from native am-Al_2O_3 films on the surface of the as-atomized Al powder (Fig. 4b). Less frequently, Al GBs free of Al_2O_3 are determined in the matrix. The core of the interfacial layer is am-Al_2O_3, while γ-Al_2O_3 crystals are formed in the vicinity of Al grains. This indicates that local devitrification of am-Al_2O_3 films on Al powders takes place during heating to the extrusion temperature of 475 °C. A similar mechanism of am-Al_2O_3 crystallization was observed by Juergens et al. [36].

The residual porosity of all materials (B, E and F) is reduced after HIP (Table 1). In Fig. 5a, the microstructure of the HIP composite F in the longitudinal direction is shown. The XRD results (Fig. 6) reveal that reaction of Ti with Al takes place during HIP to form Al_3Ti filaments (tetragonal DO_{22} structure). The Al_3Ti filaments have a length on the level of hundreds of micrometers (Fig. 5a) and consist of equiaxed grains with the size of 0.75 ± 0.17 μm (Figs. 5b, 7). A certain amount of Al_3Ti grains are located separately at the matrix-filament interface (Fig. 5b). The interface between the Al matrix and Al_3Ti filaments is clear

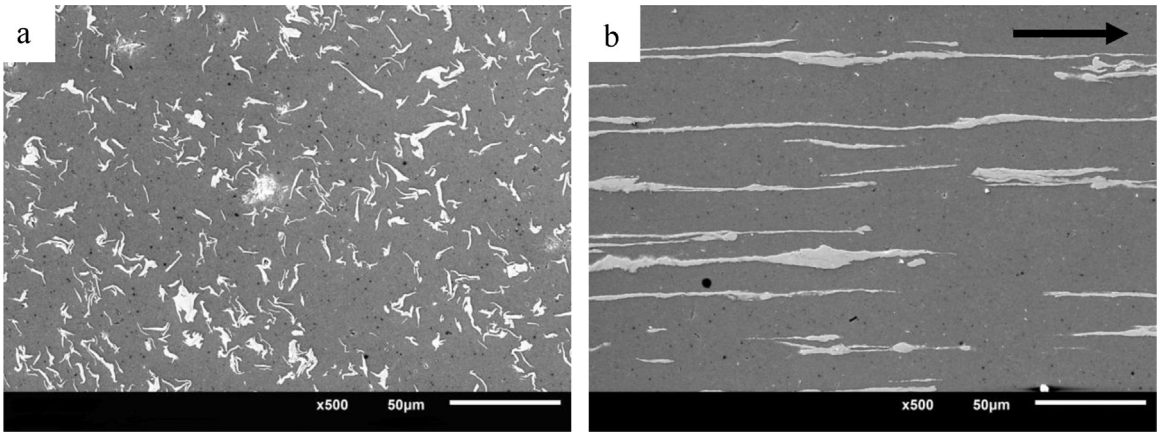

Fig. 2. SEM micrographs of the as-extruded material D in the (a) transversal and (b) longitudinal direction (the arrow shows the extrusion direction).

Table 2
The thickness of Ti and Al_3Ti filaments in composites.

Composite	Thickness of filaments (μm)
C	1.7 ± 0.6
D	1.4 ± 0.4
E	6.7 ± 2
F	9.6 ± 2.6

without any signs of voids or reactants (Fig. 8a). On the atomic level (Fig. 8b), the interface is semi-coherent with the small lattice misfit between Al and Al_3Ti (lattice misfit is -4.98% and 6.13% for *a* and *c* parameters, respectively [9,37,38]). Partially crystallized am-Al_2O_3 layers transform and crystallize into γ-Al_2O_3 particles [33,39], which reside at the Al GBs (Fig. 9). The average size of γ-Al_2O_3 particles is 28 ± 9 nm, and their content in the Al matrix is 2.4 vol% [33]. The Al grain structure of the matrix does not experience major changes upon HIP (at 600 °C for 9 h). No grain coarsening takes place during HIP and the average transversal Al grain size (0.65 ± 0.44 μm) in E and F is kept the same when compared to that of the as-extruded C and D (Fig. 3b); the portion of the LAGBs remains virtually unchanged as well (12.3%). This is clearly attributed to the presence of stable nanometric γ-Al_2O_3 particles at the GBs, which effectively stabilize Al grain structure (HAGBs and LAGBs) and prevent it from grain growth during HIP [32,33]. As demonstrated in Fig. 10, the tensile straining of Al+Al_3Ti_f MMCs accommodates multiple and intergranular fractures along the Al_3Ti filaments prior to the fracture of the composite.

3.2. Tensile properties

The 0.2% strain offset yield stress ($YS_{0.2}$) of the studied materials obtained from tensile tests at RT as a function of the volume fraction of reinforcement is shown in Fig. 11. $YS_{0.2}$ of the unreinforced matrix (material A) decreases from 224.7 to 212.8 MPa after HIP (material B). While the grain size and the portion of LAGBs remain unchanged in the as-extruded and HIP materials, the strength drop is associated with the change in morphology of the Al_2O_3 phase from the am-Al_2O_3 plates to the γ-Al_2O_3 particulates, as reported in the previous studies [29,32,33]. Despite the thin Al_3Ti layer formed at Al–Ti interfaces in C and D, Ti filaments provide no significant strength contribution. Conversely, an introduction of 15 and 30% Al_3Ti_f contributes significantly to the strengthening of composites E and F that reaches $YS_{0.2}=279.2$ and 368.8 MPa, respectively. $YS_{0.2}$ increases at the rate of 5.2 MPa per 1 vol% Al_3Ti_f. This value is comparable with the composite produced by friction stir processing studied by Hsu et al. [15], where Al+24 vol% Al_3Ti composite possesses $YS_{0.2}=383$ MPa. Fig. 12 shows the $YS_{0.2}$ of B, E and F as a function of testing temperature. The $YS_{0.2}$ for composites E and F improves at all testing temperatures compared to the unreinforced matrix B. The strengthening effect of Al_3Ti filaments is reduced with higher testing temperatures, while B, E and F possess virtually the same $YS_{0.2}=26$–36 MPa at the highest testing temperature of 600 °C. A load from matrix to filament transfers less efficiently at higher testing temperatures. The high quality of all of the fabricated samples is reflected by the very good reproducibility of achieved strengths.

The total elongation (ε_T) of the matrix B decreases with the testing temperature and reaches its minimum (~1%) at 400 °C (Fig. 12). Afterwards, it gradually increases to ~4% at 600 °C. Deterioration of the determined ε_T in the matrix B at elevated temperatures is clearly attributed to plastic instability, which has been reported for various UFG metals and composites [32,33,40–44]. Plastic instability occurs due to a large surface area of HAGBs and the low content of mobile dislocations, which results in reduced strain hardening, the yield drop phenomenon and the formation of necking just after yielding (Fig. 13). The existence of necking at the early stage of deformation renders proper determination of ε_T from stress–strain curves and eventually penalizes the ductile matrix B with lower ε_T at elevated temperatures. Plastic instability (i.e., the dislocation annihilation at grain boundaries) is governed by thermally activated processes and is therefore pronounced at higher temperatures and at smaller strain rates [30,43,44]. The reason that ε_T of the matrix B increases at temperatures >400 °C remains unclear. The presence of brittle Al_3Ti filaments is associated with the low ε_T of ~1% of composites E and F at temperatures ≤ 400 °C (Fig. 12). This contrasts with the reasonably good $\varepsilon_T=11$–12% of unreinforced B, which contains 2 vol% of γ-Al_2O_3, at temperatures <400 °C. The ε_T of composites improves gradually above 400 °C. Apparently, the Al_3Ti filaments improve ε_T at temperatures >400 °C, which increases compared to unreinforced matrix B. This becomes especially pronounced at 600 °C, where composite F with 30% Al_3Ti_f reaches the highest $\varepsilon_T=\sim 11\%$, which is more than composite E with 15% Al_3Ti_f (~6%) and matrix B (~4%). Brittle Al_3Ti filaments in E and F composites disintegrate during straining prior to fracture (Fig. 10). This finding indicates that Al_3Ti filaments contribute to the load transfer only in the early stages of the tensile straining. It is assumed that Al_3Ti filaments help to prevent the localization of plastic deformation in the UFG Al matrix in an early stage of tensile deformation [41,42].

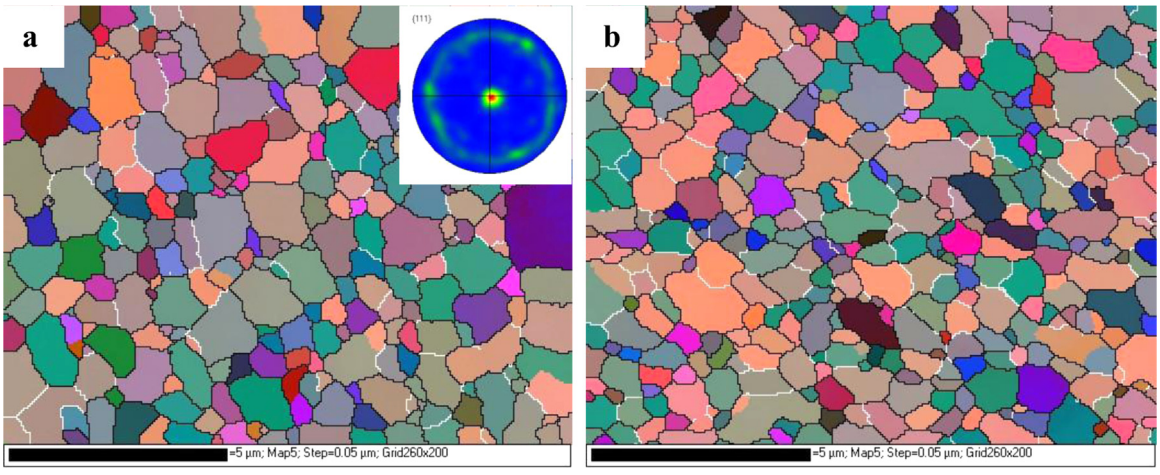

Fig. 3. The grain orientation map of the Al matrix in the (a) as-extruded D with an inset showing the {111} plane pole figure and the (b) HIP composite F, both shown in the transversal direction. The white and black lines in maps represent LAGBs (3–15°) and HAGBs (> 15°) of Al grains, respectively.

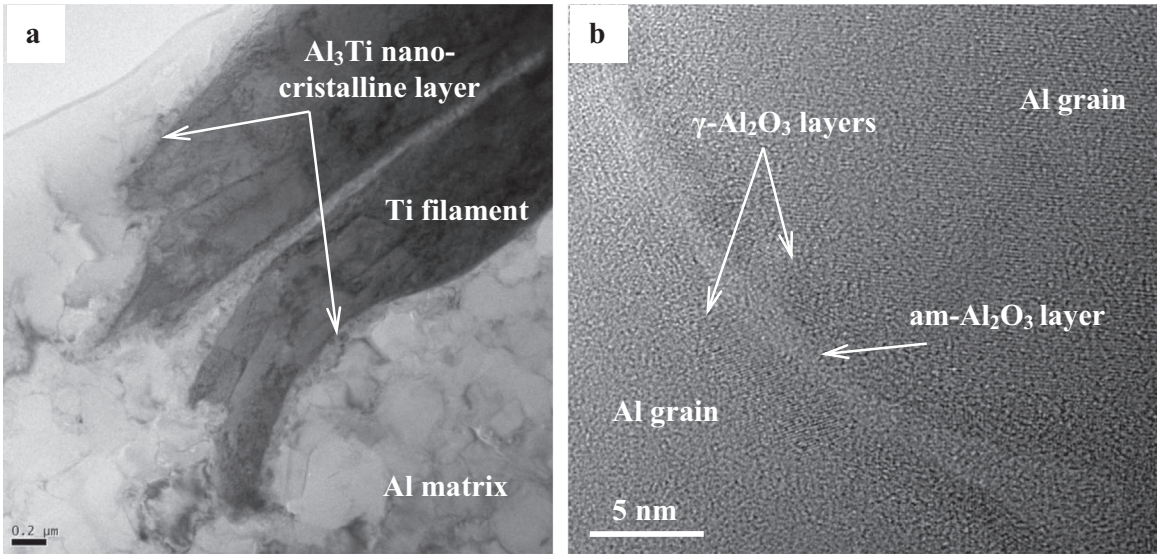

Fig. 4. TEM detail of the (a) interface between the Al matrix and Ti filament, and (b) two adjacent grains in the Al matrix in the as-extruded D composite.

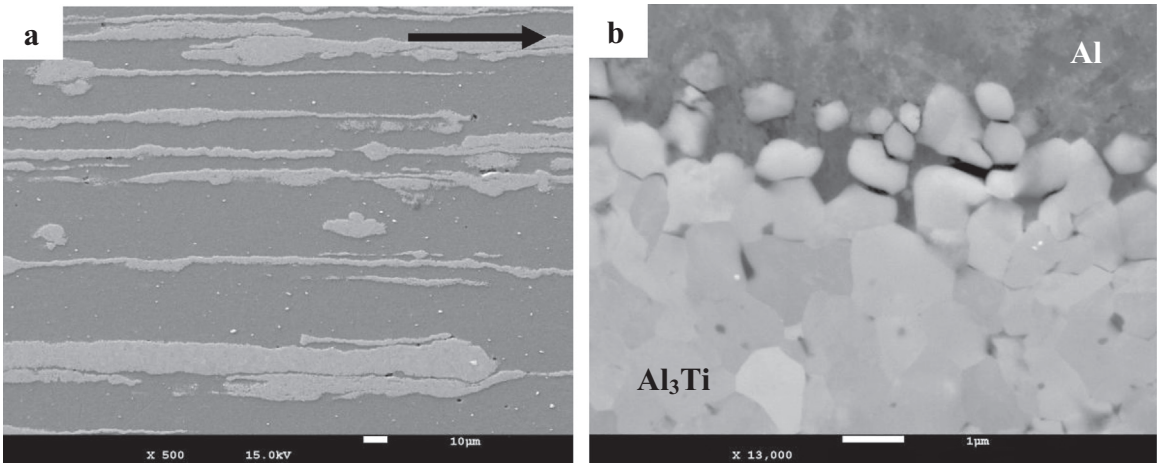

Fig. 5. SEM micrograph of the composite F in the (a) longitudinal direction (the arrow represents the extrusion direction) and the (b) Al–Al_3Ti interface detail.

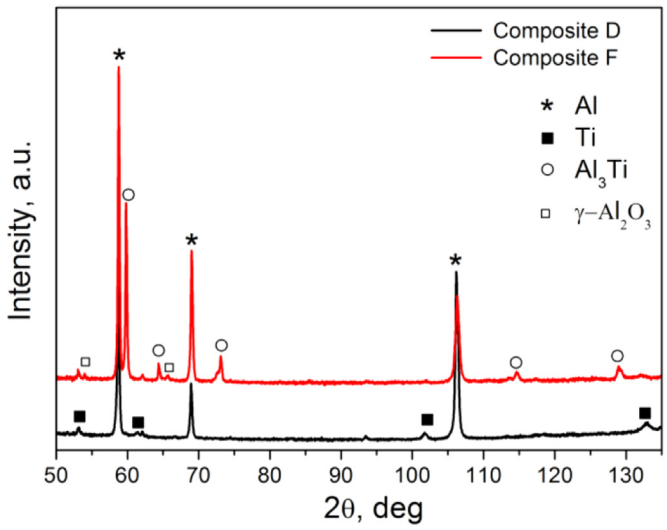

Fig. 6. XRD patterns of the as-extruded D and HIPed composite F.

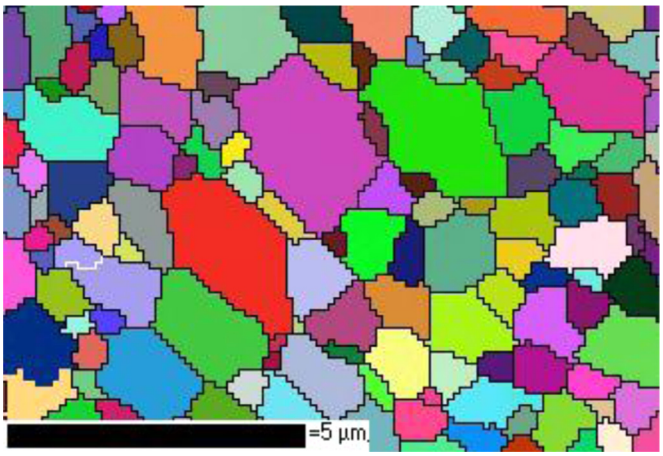

Fig. 7. The grain orientation map of the Al_3Ti filament in the composite F shown in the longitudinal direction.

The yield drop phenomenon becomes less significant for composites E and F tested at elevated temperatures (Fig. 13). Thus, by introduction of Al_3Ti filaments, the ductility potential of the UFG Al matrix is harnessed for the entire volume of the tensile bar gauge. Moreover, the Al-Al_3Ti interfaces act as a dislocation source that further promotes the ductility of composites at elevated temperatures. Consequently, composites E and F reach higher ductility than the matrix at $>400\,^{\circ}C$.

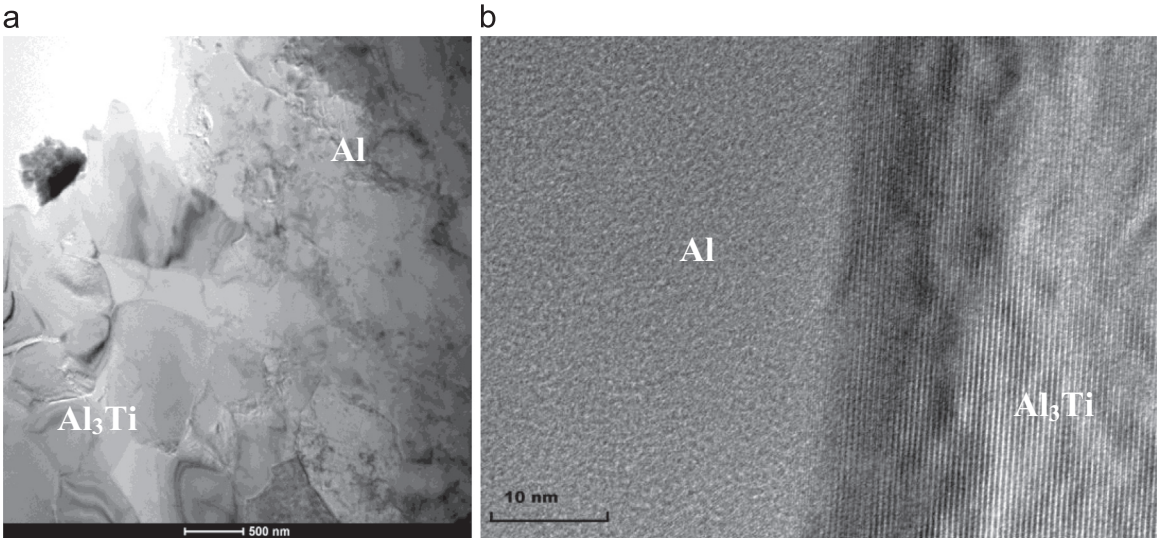

Fig. 8. (a) TEM image and (b) HRTEM detail of the interface between the Al matrix and Al_3Ti filament in the composite F shown in the transversal direction.

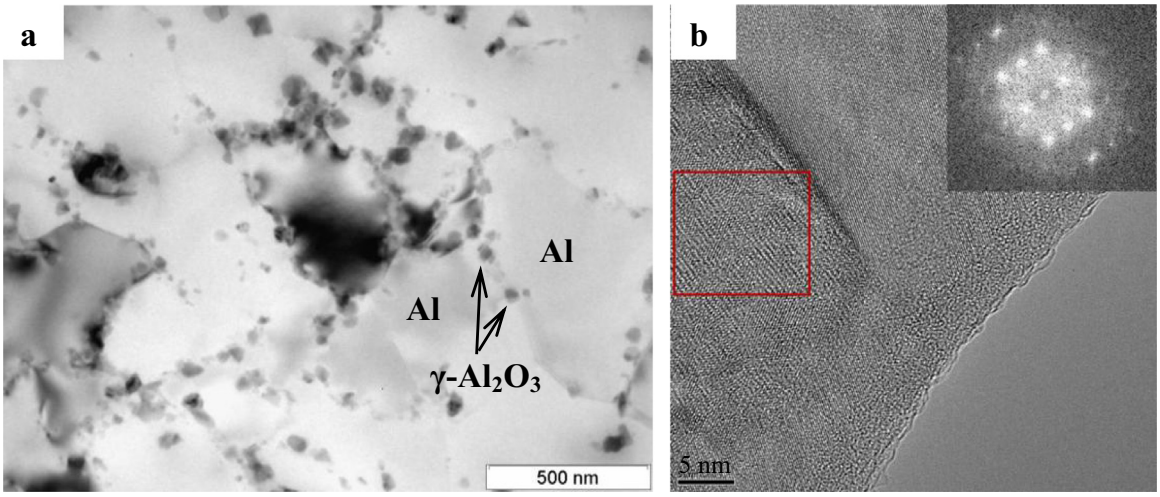

Fig. 9. (a) TEM image of nanometric γ-Al_2O_3 particles at the Al GBs of the matrix area in the HIP composite F. HRTEM detail of the γ-Al_2O_3 particle with corresponding FFT.

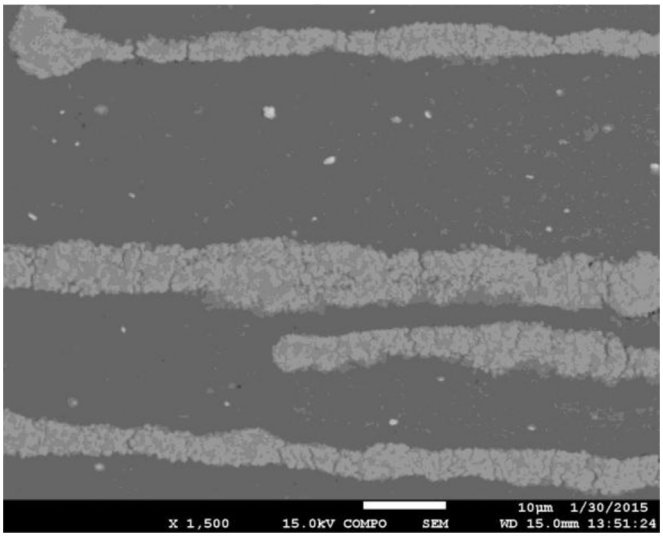

Fig. 10. SEM micrograph of the composite F strained to 5% at a temperature of 600 °C.

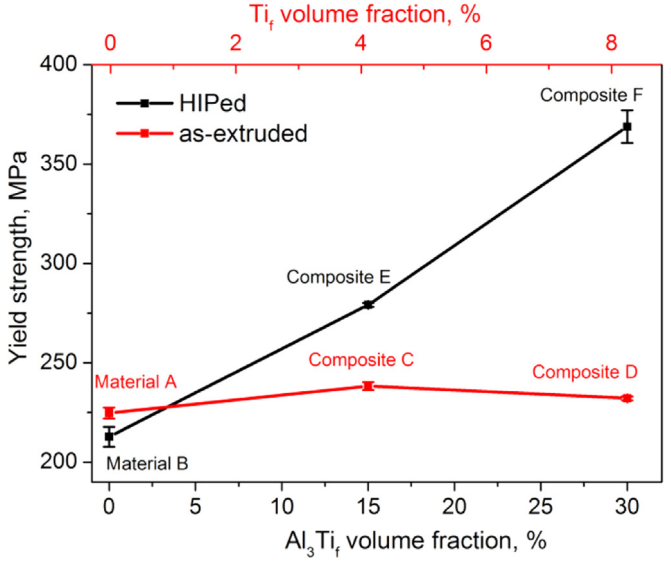

Fig. 11. The yield strength of composites C, D, E, and F and matrix materials A and B at room temperature.

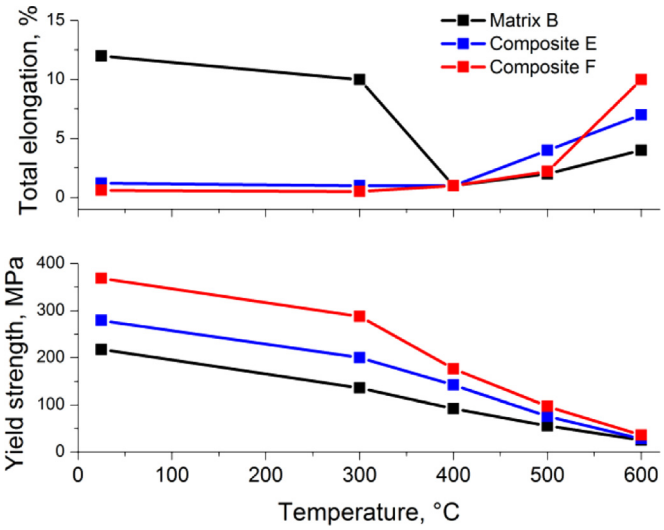

Fig. 12. The yield strength and the total elongation of composites E and F and matrix B as a function of the testing temperature.

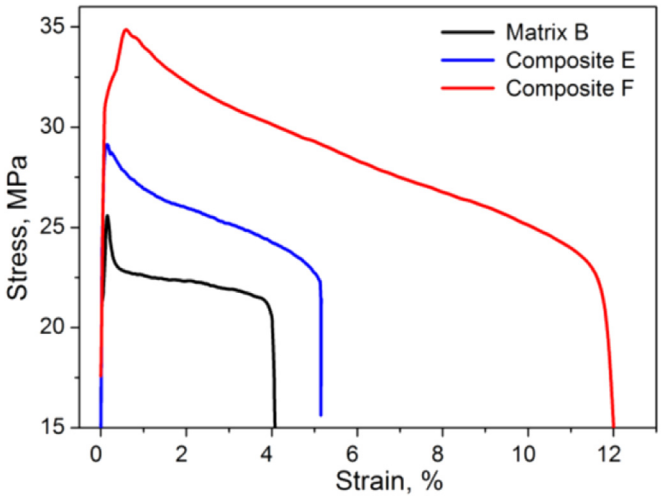

Fig. 13. The engineering stress–strain curves of matrix B and composites E and F tested at 600 °C.

3.3. Young's modulus

The presence of stiff Al_3Ti filaments significantly increases the YM of composites (Fig. 14). For instance, composite F with 30% of Al_3Ti_f reaches a high value YM = 107.4 GPa. The YM of the composites lie slightly below the theoretical line, as given by the rule of mixtures. This small deviation is attributed to the Al_3Ti grains at the interface with the Al matrix, which are separated from a filament core. Experimental data are in accordance with the Halpin–Tsai model defined by the formulae [45]:

$$YM_c = YM_m \frac{1+\xi\eta V_f}{1-\eta V_f},\ \eta = \frac{YM_f/YM_m - 1}{YM_f/YM_m + \xi},\ \xi = 2\frac{l_f}{d_f} \quad (2)$$

where YM_m and YM_f are Young´s moduli of the matrix and filaments, respectively. V_f is the volume fraction, and d_f is the average diameter (i.e., thickness) of the filaments. The average length of the filaments (l_f) is assumed to be ~300 μm. YM of E and F determined at RT increases at a rate of 1.25 GPa per 1 vol% Al_3Ti, which agrees well with other Al–Ti alloys prepared by rapid solidification and mechanical milling [14,46]. The evolution of YM for the composites in the range of RT to 550 °C is shown in Fig. 15. For the unreinforced matrix B, YM decreases almost linearly in the

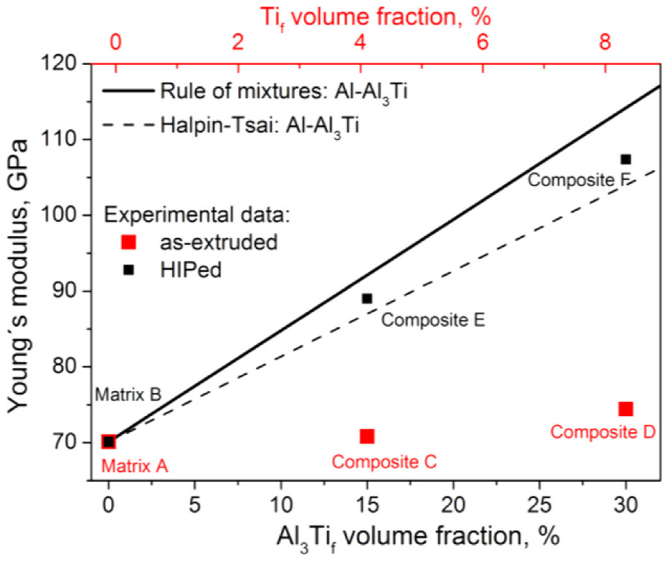

Fig. 14. The Young's modulus of composites C, D, E, and F and matrix materials A and B measured at room temperature as a function of the reinforcement volume fraction.

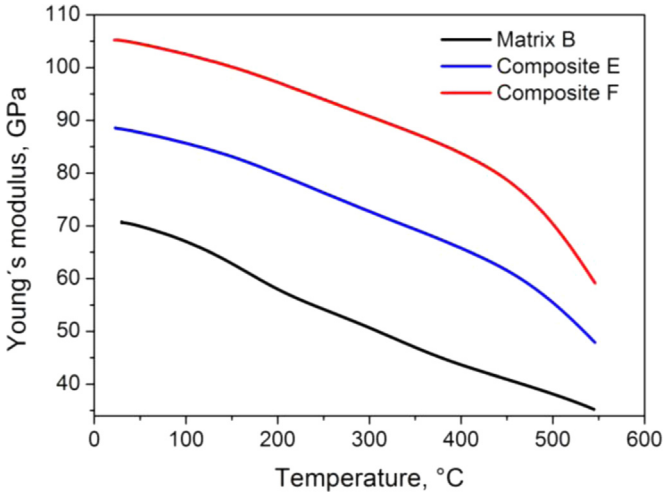

Fig. 15. The Young's modulus of composites E and F and matrix B as a function of temperature.

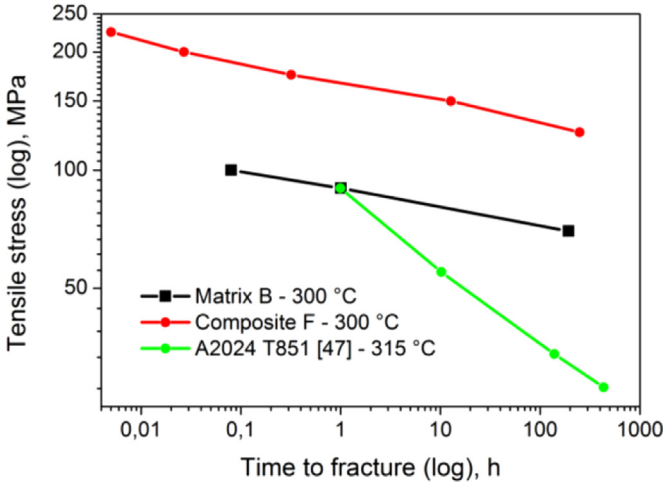

Fig. 16. Stress – time to rupture plot of composite F and matrix B subjected to tensile creep tests at 300 °C. For comparison, data of reference A2024 T851 alloy [48] are shown.

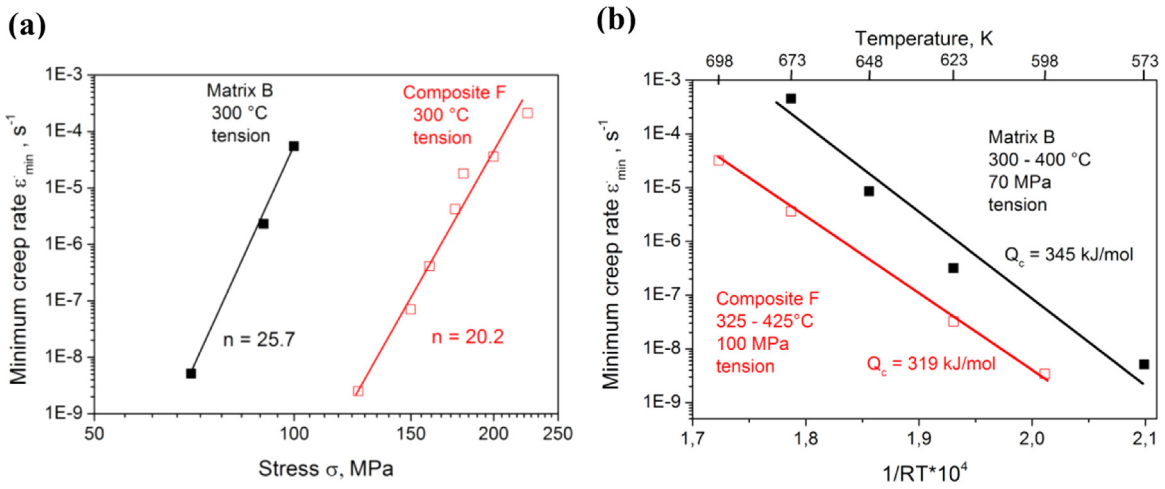

Fig. 17. (a) The minimum creep rate - applied tensile stress plots and (b) Arrhenius plot of composite F and matrix B.

measured temperature range. For composites E and F, the YM starts decreasing more steeply at ~450 °C, while this tendency becomes more pronounced with a higher content of Al_3Ti. This is assumed to be due to the decrease in residual stresses caused by the mismatch between coefficients for thermal expansion (CTE) of Al (CTE at 22 °C: 22.10^{-6} °C^{-1} [28]) and Al_3Ti (CTE at 22 °C: 13.10^{-6} °C^{-1} [47]), and by the difference between the processing and given temperatures.

3.4. Creep properties

Composite F shows a significantly improved creep performance over the ingot Al–Cu–Mg-based precipitation hardened A2024 T851 alloy, the thermally stable reference alloy used for combustion engine pistons [48] (Fig. 16). This behavior is due to the UFG Al matrix stabilized with nanoscale γ-Al_2O_3 and strengthened with directional Al_3Ti filaments formed *in situ*. Fig. 17a shows the variation of the measured minimum creep rate (ε_{min}) with the applied stress for material B and composite F at a temperature of 300 °C. It is found that both unreinforced B and reinforced F exhibit no significant differences in the values of the stress exponent (n) as well as the creep activation energy (Q_C) (Fig. 17). These results indicate that the creep deformation of both the matrix and composite is controlled by a similar creep mechanism. Slightly lower values of n and Q_C of composite F can be attributed to the presence of Al_3Ti filaments with micrometric size, which act as a dislocation source [49,50]. The results show that the ε_{min} of composite F are two or three orders of magnitude lower than those of the unreinforced matrix B at the same conditions; thus, the creep resistance is markedly improved. This means that the interaction between dislocations and Al_3Ti filaments in the matrix alloy plays a significant role in the creep strengthening of the composite. Both B and F materials exhibit a high value of n and Q_C. The values of n are much higher than those of the cast pure Al or solid solution strengthened Al alloys (n=3–5). Furthermore, Q_C greatly exceeds the lattice self-diffusion of Al (142 kJ mol^{-1}). Similar behavior is reported in several works related to PM Al materials [51–53]. Park et al. [52] show that both unreinforced and reinforced PM A6061 alloys exhibit high and variable n and Q_C. This result indicates that the creep behavior of examined materials is analogous to one of the dispersion strengthened alloys (DSA). Higher creep performance of DSA is related to the interaction between moving dislocations and oxide particles, which are present in Al grains as a result of PM processing. Requena et al. confirm the key importance of Al_2O_3 dispersoids, formed *in situ* as a result of native Al_2O_3 films on Al powders, on the creep performance of the *ex-situ* PM Al+SiC_p composite [49]. The effect of different morphologies (particles, layers or continuous network) of the *in-situ* Al_2O_3 phase, which resides on the Al HAGBs, on the creep behavior of the UFG Al is currently under investigation [54].

4. Conclusions

In-situ UFG Al-(15, 30 vol%) Al_3Ti composites were prepared by extrusion of Al–Ti powder mixtures followed by solid-state reactive diffusion during HIP operation. The microstructure and properties were systematically investigated, with emphasis placed on the performance at elevated temperatures. The following important conclusions were made:

Fine Al powder (d_{50}=1.3 μm) deforms coarser Ti powder particles (d_{50}=24.5 μm) into micrometric filaments during extrusion.

Solid-state reactive diffusion by HIP yields *in-situ* formation of Al_3Ti filaments embedded in a pore-free Al matrix. In parallel, nanometric γ-Al_2O_3 particles (2.4%) form *in situ* at Al HAGBs as a result of fractured native am-Al_2O_3 films on Al powders.

The γ-Al_2O_3 particles effectively stabilize Al grain structure and prevent it from experiencing grain growth during HIP.

The presence of *in-situ* directional Al_3Ti filaments significantly improves the strengths ($YS_{0.2}$ up to 368.8 MPa) and the Young`s moduli (YM up to 107.4 GPa) of the composites. The $YS_{0.2}$ and YM increase at rates of 5.2 MPa and 1.25 GPa per 1 vol% Al_3Ti, respectively. The composites possess excellent $YS_{0.2}$ and YM at elevated temperatures.

The UFG Al matrix with embedded nanometric γ-Al_2O_3 particles results in excellent creep performance. The introduction of microsize Al_3Ti filaments into the UFG Al matrix leads to a further significant reduction in the minimum creep rate.

The Al_3Ti filaments help to prevent the localization of plastic deformation in the UFG Al matrix, and thus, elongation of composites improves at elevated temperatures compared to unreinforced Al matrix.

Acknowledgments

Financial support from the SRDA APVV-0556-12 project, the SAS-NSC JRP 2011/06 project, the CONICET-SAS RD no 182/13 project, CEITEC CZ.1.05/1.1.00/02.0068 project and the VEGA 2/0025/14 and 2/0065/16 projects is gratefully acknowledged. The authors thank Ivo Vavra from IEEE SAS for help with TEM characterization and Peter Svec from IP SAS for the XRD analysis.

References

[1] D.B. Miracle, Compos. Sci. Technol. 65 (2005) 2526–2540.
[2] F.A. Girot, J.M. Quenisset, R. Naslain, Compos. Sci. Technol. 30 (1987) 155–184.
[3] T.W. Chou, A. Kelly, A. Okura, Composites 16 (1985) 187–206.
[4] M. Nakamura, K. Kimura, J. Mater. Sci. 26 (1991) 2208–2214.
[5] J. Wang, S.L. Shang, Y. Wang, Z.G. Mei, Y.F. Liang, Y. Du, Z.K. Liu, Calphad 35 (2011) 562–573.
[6] S.H. Wang, P.W. Kao, Acta Mater. 46 (1998) 2675–2682.
[7] Z. Liu, Q. Han, J. Li, Powder Technol. 247 (2013) 55–59.
[8] K. Das, L.K. Narnaware, Mater. Sci. Eng. A 497 (2008) 25–30.
[9] X. Wang, A. Jha, R. Brydson, Mater. Sci. Eng. A 364 (2004) 339–345.
[10] V. Abbasi Chianeh, H.R. Madaah Hosseini, M. Nofar, J. Alloy. Compd. 473 (2009) 127–132.
[11] R. Lerf, D.G. Morris, Mater. Sci. Eng. A 128 (1990) 119–127.
[12] S.S. Nayak, S.K. Pabi, B.S. Murty, J. Alloy. Compd. 492 (2010) 128–133.
[13] S. Srinivasan, S.R. Chen, R.B. Schwarz, Mater. Sci. Eng. A 153 (1992) 691–695.
[14] Y.C. Cheng, S.H. Wang, P.W. Kao, C.P. Chang, Mater, Sci. For. 217 (1996) 1891–1900.
[15] C.J. Hsu, C.Y. Chang, P.W. Kao, N.J. Ho, C.P. Chang, Acta Mater. 54 (2006) 5241–5249.
[16] Q. Zhang, B.L. Xiao, Z.Y. Ma, Mater. Chem. Phys. 139 (2013) 596–602.
[17] Q. Zhang, B.L. Xiao, D. Wang, Z.Y. Ma, Mater. Chem. Phys. 130 (2011) 1109–1117.
[18] Q. Zhang, B.L. Xiao, P. Xue, Z.Y. Ma, Mater. Chem. Phys. 134 (2012) 294–301.
[19] Y. Mishin, C.H.R. Herzig, Acta Mater. 48 (2000) 589–623.
[20] I.C. Barlow, H. Jones, W.M. Rainforth, Acta Mater. 49 (2001) 1209–1224.
[21] I.C. Barlow, H. Jones, W.M. Rainforth, Mater. Sci. Eng. A351 (2003) 344–357.
[22] G.X. Wang, M. Dahms, G. Leitner, S. Schultrich, J. Mater. Sci. 29 (1994) 1847–1853.
[23] M. Dahms, Mater. Sci. Eng. A 110 (1989) L5–L8.
[24] M. Dahms, S. Schwantes, Mater. Sci. Eng. A 151 (1992) L27–L29.
[25] L. Xu, Y.Y. Cui, Y.L. Hao, R. Yang, Mater. Sci. Eng. A 435–436 (2006) 638–647.
[26] M. Balog, J. Nagy, K. Izdinsky, F. Simancik, Int. J. Mater. Prod. Technol. (2005) 69–78.
[27] M. Balog, J. Nagy, F. Simancik, K. Izdinsky, G. Requena, Rev. Adv. Mater. Sci. 18 (2008) 415–421.
[28] M. Balog, F. Simancik, O. Bajana, G. Requena, Mater. Sci. Eng. A504 (2009) 1–7.
[29] M. Balog, C. Poletti, F. Simancik, M. Walcher, W. Rajner, J. Alloy. Compd. 509S (2011) S235–S238.
[30] C. Poletti, M. Balog, F. Simancik, H.P. Degischer, Acta Mater. 58 (2010) 3781–3789.
[31] M. Balog, F. Simancik, M. Walcher, W. Rajner, C. Poletti, Mater. Sci. Eng. A 529 (2011) 131–137.
[32] M. Balog, P. Krizik, M. Nosko, Z. Hajovska, M.V. Castro Riglos, W. Rajner, D. S. Liu, F. Simancik, Mater. Sci. Eng. A 613 (2014) 82–90.
[33] M. Balog, T. Hu, P. Krizik, M.V.C. Riglos, B.D. Saller, H. Yang, J.M. Schoenung, E. J. Lavernia, Mater. Sci. Eng. A 648 (2015) 61–71.
[34] E.E. Underwood, Quantitative stereology, Addison-Wesley, Reading, 1970.
[35] A.M. Russell, T. Lund, L.S. Chumbley, F.A. Laabs, L.L. Keehner, J.L. Harringa, Compos. Part A -Appl. Sci. Manuf. 30 (1999) 239–247.
[36] L.P.H. Jeurgens, W.G. Sloof, F.D. Tichelaar, E.J. Mittemeijer, Thin Solid Films 418 (2002) 89–101.
[37] S. Saha, T.Z. Todorova, J.W. Zwanziger, Acta Mater. 89 (2015) 109–115.
[38] P. Norby, A.N. Christensen, Acta Chem. Scand. Ser. A 40 (1986) 157–159.
[39] R. Casati, A. Fabrizi, A. Tuissi, K. Xia, M. Vedani, Mater. Sci. Eng. A 648 (2015) 113–122.
[40] Y.M. Wang, E. Ma, Acta Mater. 52 (2004) 1699–1709.
[41] G. He, W. Loeser, J. Eckert, L. Schultz, Nat. Mater. 2 (2003) 33–37.
[42] E. Ma, Nat. Mater. 2 (2003) 7–8.
[43] C.Y. Yu, P.W. Kao, C.P. Chang, Acta Mater. 53 (2005) 4019–4028.
[44] N. Kamikawa, X. Huang, N. Tsuji, N. Hansen, Acta Mater. 57 (2009) 4198–4208.
[45] J.C. Halpin, Primer on composite materials: Analysis, Rev.edn, Technomic Publishing Co, Lancaster, PA, 1984.
[46] J.M. Wu, S.L. Zheng, Z.Z. Li, Mater. Sci. Eng. A 289 (2000) 246–254.
[47] T. Li, E.A. Olevsky, M.A. Meyers, Mater. Sci. Eng. A 473 (2008) 49–57.
[48] J.G. Kaufman, Parametric Analyses of High-temperature Data for Aluminium Alloys, 1st ed, ASM International, Ohio, 2008.
[49] G. Requena, B. Bauer, H.P. Degischer, M. Lieblich, Int. J. Mater. Res. 102 (2011) 982–992.
[50] F.A. Mohamed, Mater. Sci. Eng. A 245 (1998) 242–256.
[51] A.B. Pandey, R.S. Mishra, Y.R. Mahajan, Acta Mater. 45 (1997) 1297–1306.
[52] K.T. Park, E.J. Lavernia, F.A. Mohamed, Acta Met. Mater. 42 (1994) 667–678.
[53] L. Kloc, S. Spigarelli, E. Cerri, E. Evangelista, Acta Mater. 45 (1995) 529–540.
[54] G. Requena, A. Sikora, M. Balog, P. Krizik, Creep testing of forged, extruded and HIP processed HITEMAL materials, unpublished results.